

Cluster Mergers as Triggers of Star Formation and Radio Emission: A Comparative Study of the Rich Clusters A2125 and A2645

Frazer N. Owen¹

*National Radio Astronomy Observatory²
Socorro, New Mexico 87801*

Michael J. Ledlow¹

*University of New Mexico, Dept. of Physics & Astronomy
Albuquerque, NM 87131*

William C. Keel¹

*University of Alabama, Dept. of Physics and Astronomy
Tuscaloosa, AL*

and

Glenn E. Morrison^{1, 3}

*University of New Mexico, Dept. of Physics & Astronomy
Albuquerque, NM 87131*

¹Visiting Astronomer, Kitt Peak National Observatory, National Optical Astronomy Observatories, operated by the Association of Universities for Research in Astronomy, Inc., under contract with the National Science Foundation.

²The National Radio Astronomy Observatory is operated by Associated Universities, Inc., under a cooperative agreement with the National Science Foundation.

³ Also National Radio Astronomy Observatory, P. O. Box O, Socorro, NM 87801.

ABSTRACT

We report a detailed optical study of the clusters Abell 2125 and 2645. These clusters are very similar in redshift ($z \approx 0.25$) and richness (Abell class 4), yet contrast strongly in blue fraction and radio-galaxy populations. Butcher & Oemler (1984) report that A2125 and A2645 have blue-galaxy fractions of 0.19 and 0.03 respectively, while radio observations with the VLA and subsequent optical identifications on the digital Palomar Sky Survey show an apparent excess of radio galaxies in A2125 relative to A2645 (Dwarakanath & Owen 1996).

Our spectroscopic observations confirm this difference. We find 27 radio galaxies to be members of A2125, and only four in A2645, based on (nearly) complete observations to the same limiting magnitude and radio flux density. The radio galaxies in A2125 extend over about 5 Mpc (assuming $H_0 = 75 \text{ km s}^{-1} \text{ Mpc}^{-1}$) along a band running from

NE to SW of the cluster center. About half the radio galaxies are red and have optical spectra which resemble old stellar populations. The other half are blue with emission lines, most of which indicate an origin in star formation rather than AGN. Many of the blue galaxies are located in a distinct clump located about 2 Mpc in projection from the cluster center.

The excess population of radio galaxies in A2125 occurs entirely at radio luminosities $< 10^{23} \text{ W Hz}^{-1}$, where one expects star-formation to be primarily responsible for the radio emission. Most of these radio galaxies have optical properties most consistent with systems later than E/S0. However, the optical line luminosities are often weaker than one would expect for the star formation rates implied by the radio emission. Thus we suspect that dust obscuration, larger than is usually found locally, hides most of the star-forming regions optically.

The existence of a cluster-cluster merger in progress in A2125 seems likely to play some role in these phenomena, although the details are obscure.

Subject headings: galaxies: active—galaxies: clusters: individual (Abell 2125, Abell 2645)—galaxies: distances and redshifts—galaxies: evolution—galaxies: kinematics and dynamics—galaxies: photometry—galaxies: starburst

1. Introduction

One of the strongest observational signatures of galaxy evolution is the Butcher-Oemler (BO) effect (Butcher & Oemler (1984)), an increase in the fraction of blue galaxies found in rich clusters with increasing redshift. This largely indicates that star formation was more active in these clusters in the past than it is now. However, the BO definition of “blue” is relative to the populous red cluster members, objects whose colors indicate little star formation within the $\sim 10^9$ years before the epoch of observation. Most studies of the BO effect in clusters have concentrated on the cores, for the practical reason that foreground or background contamination is least important and most easily corrected there. However, many of the proposed mechanisms to mediate the BO effect, and hence the overall evolution of galaxies in the cluster environment, have effects spread across the cluster, and in some cases predict different behavior far from the core. Thus if one could study cluster populations further from the cluster center as well as closer to the epoch of the star formation, one might expect to learn more about the origins of the BO effect.

Tracing star formation might be done most ideally via far-infrared mapping, since some star formation can be hidden by surrounding dust. This remains difficult due to instrumental field-of-view and sensitivity limitations, but the well-established relation between far-IR and centimeter radio fluxes for galaxies means that radio surveys can serve as a useful surrogate for such IR data. Below $10^{23} \text{ W Hz}^{-1}$, the radio-galaxy luminosity function is dominated by emission from galaxies driven by star formation. The VLA at 20cm has a field of view of 30 arcmin (FWHM) and can detect radio sources down to about $10^{22} \text{ W Hz}^{-1}$ out to $z = 0.4$. Since the radio sky is much less crowded at these levels than in a deep optical image, the optical identifications of galaxies bright enough to be giant systems at the redshift of a cluster are very likely to be associated with clusters at redshifts as large as 0.4.

In this paper we report optical observations of the bright radio ID’s found in two clusters, A2125 and A2645 imaged with the VLA at 20cm. The radio observations are reported by Dwarakanath & Owen (1999). These two clusters were chosen as examples of rich systems studied by Butcher & Oemler (1984). Both are richness class 4 clusters and both have redshifts of ~ 0.25 . However, A2125 has a large blue fraction (0.19 ± 0.03) while A2645 has a much smaller

blue fraction (0.03 ± 0.05). Does this difference in blue fraction translate into a corresponding difference in the radio galaxy population? Initial results for this project showed a large excess of radio galaxies in Abell 2125 compared with A2645 (Dwarakanath & Owen 1996, Owen 1996, Owen et al., 1996). Now we consider the situation in more detail using new observations. Below we report both optical imaging and spectroscopy of the radio identifications found in the directions of these two clusters.

2. Observations and Reductions

In August 1995 we imaged Abell 2125 and Abell 2645 with the KPNO 0.9m telescope in B and Cousins R. The CCD detector was a 2048X2048 Tektronics chip with a pixel size on the sky of 0.68 arcsec. Four twenty minute, dithered exposures were stacked for both R images. In B one five minute exposure was obtained for A2645 and a ten-minute exposure for A2125. All frames were bias corrected and flattened using a twilight frame. Each frame was calibrated using about 20 standard stars (Landolt 1983, Landolt 1992), bootstrapping from a shorter observation from a photometric night if the calibration for the longer integration was questionable. Acceptable calibration nights had rms errors in the derived transformations of < 0.03 magnitudes. The *B*-band data from A2125 were supplemented by a 20-minute exposure at the prime focus of the KPNO 4m Mayall telescope using a similar filter/CCD combination, calibrated using stars from the M92 field reported by Christian et al (1985). Also in November, 1998, Elizabeth Rizza obtained a deeper B frame of A2645 for us with one hour total integration using the 0.9m with the same CCD and filter as our earlier observation. We have used our five minute, well-calibrated B frame to bootstrap the calibration to the deeper image and the colors we report for A2645 come from this image.

The R observations transformed well without a color term to Cousins R; however, the B observations from the 0.9m telescope needed an 8.6% *B - R* color correction to match the Johnson B standard stars. This color term is not well matched to redshifted galaxy energy distributions and thus we have calculated the B magnitudes in the instrumental system by using the Johnson B zero point for *B - R* = 0. The instrumental filter + CCD response has been calculated by Morrison 1999 from the KPNO response curve and this B system has been used in all model

spectra calculations we have performed. For the 4-m data, we have included correction for a mild color term (0.04 magnitude in B per unit of $B - R$).

We have adopted the Gunn-Oke (Gunn & Oke 1981) metric aperture for measuring galaxy magnitudes. For our adopted cosmology ($H_0 = 75 \text{ km s}^{-1}$ and $q_0 = 0.1$), this corresponds to a radius of 13.1 kpc (3.8 arcsec for $z = 0.25$). This has the advantage of containing almost all the light for galaxies with luminosities $\leq L_*$ (Ledlow & Owen 1995) while being small enough to minimize the error due the sky background and in most cases avoiding contamination by nearby objects in the aperture.

Magnitudes and internal errors were calculated using the IRAF task PHOT. A calibration error of 0.05 magnitudes was adopted as an estimate of the total photometric calibration error, including the transformation, any systematic error associated with the individual observation and any systematic background errors. The errors in the R magnitudes are all dominated by these external terms and an error of 0.05 magnitudes is adopted for all R observations. The color errors for faintest objects are sometimes dominated by the counting statistics in B exposure. Thus for the colors we have quoted an error combining both the counting and the calibration errors.

Spectra of the radio-galaxy identifications were obtained in June 1995 and May 1996, using a long slit on the KPNO 4m Mayall telescope with the RC spectrograph. The grating had 316 lines/mm, blazed at 4000\AA . In 1995, the program was primarily intended for high-redshift radio galaxies and we covered the wavelength range $3500\text{--}7000\text{\AA}$ for this purpose. In 1996 we chose a redder wavelength region of $4300\text{--}8600\text{\AA}$ to cover both the 3727\AA [O II] line and the the [N II]/H α complex in the restframe of a $z = 0.25$ cluster. For the 1996 observations, we used the Risley prisms for atmospheric dispersion compensation, allowing more freedom in selecting a position angle for the slit without compromising signal in the blue. Slit widths $1.5\text{--}2''$ were used, for the best contrast between galaxy and night-sky light at the relevant angular sizes. When possible, the long slit was rotated so that two radio galaxies or a radio galaxy and an apparent companion could be covered in a single exposure of 5–15 minutes. Standard stars were observed each night to calibrate the shape of the spectral energy distribution for each galaxy, although no absolute calibration was attempted. Comparison of photometric and spectroscopically synthesized (B-R)

values shows that the flux calibration is consistent for continuum shape and line ratios at better than the 10% level from $4500\text{--}7000 \text{\AA}$.

Redshifts were obtained using the IRAF task, FXCOR, with a K0 III radial velocity standard as the template. The calibration errors were estimated using radial velocity standards observed on different nights and was found to be $\leq 20 \text{ km s}^{-1}$. Thus the errors are dominated by the individual spectral S/N. Without a large database to further evaluate errors, we have adopted the quoted errors from FXCOR.

3. Results from Radio & Optical Observations

The optical identification process is described in Dwarakanath & Owen (1999). Our spectroscopy is complete for radio identifications in these clusters among galaxies brighter than Gunn-Oke $M_R = -21.0$, except for four objects in A2645 and one in A2125 which would be brighter than this limit if they were at the cluster redshift. In table 1 and 2, we summarize the magnitudes, colors, and heliocentric redshifts for each galaxy. An “e” appended to the redshift indicates the redshift is based on an emission line spectrum. Errors are quoted in parenthesis. Some of our radio galaxies lie outside the area covered by the CCD frames. Magnitudes for these objects, estimated from the Digital Sky Survey with rough calibration from our CCD images, are given in parenthesis without any errors.

In table 3, we present more detailed information for each cluster member in A2125 and A2645 with spectroscopy: absolute Gunn-Oke R magnitude, B-R color, D(4000), log of the absolute radio luminosity, and for fairly isolated galaxies, a mean surface brightness and concentration index (Abraham et al 1994). In this table we have corrected the magnitudes and colors for galactic extinction using the results of Burstein & Heiles 1981 and applied a K-correction (Morrison 1999). The surface brightness have been corrected for $(1+z)^4$ cosmological dimming as well.

In table 4, we summarize the emission-line luminosities and calculated star formation rates for the A2125 members. In calculating the line luminosities we have assumed that the line emission is actually spread throughout the entire galaxy rather than concentrated only in the nuclear region sampled by the slit. To make this correction, we adjusted the absolute calibration of the spectra to match the Gunn-

Oke aperture magnitudes calculated from the direct images. The spectra were dereddened for galactic extinction, and K-corrections were estimated individually for each galaxy by comparing the flux over the B and R bandpasses for the galaxy in the observed frame and artificially shifted to zero redshift. The K-corrections derived in this way are in reasonable agreement with Frei & Gunn (1994) over the range of galaxy morphologies in our sample based on the concentration parameters listed in table 3.

4. Velocity Field and Mean Cluster Redshifts

Very few redshifts besides those presented here have been published for these two clusters. For A2645, Newberry, Kirshner, & Boroson (1988) measured five cluster galaxies with adequate accuracy to use for an estimate of the cluster mean velocity. One object is in common with our results and agrees well within the estimated errors. In figures 1 and 2, we show the velocity distributions near $z = 0.25$ from our data, including Newberry, Kirshner, & Boroson (1988) for A2645. For both clusters, there is a concentration near 0.25. For the combined sample for A2645, we find a mean velocity of 0.2500 ± 0.0020 . For A2125, we find a biweight scale (dispersion) of 891 km sec^{-1} and a biweight mean of 0.2460 ± 0.0007 . In A2125 there are three galaxies with redshifts near 0.275. These galaxies do not survive a 3σ clipping with the calculated dispersion. Thus we find 27 radio identifications consistent with cluster membership in A2125. We adopt these mean redshifts for our further analysis of each cluster.

5. Optical and X-ray Properties of A2125 and A2645

In figures 3 and 4, we show the R optical images of A2125 and A2645 with contours of the X-ray emission superimposed. The A2125 X-ray image is from the *ROSAT* PSPC while the A2645 X-ray results are from *ROSAT* HRI. The sensitivity of the HRI image of A2645, smoothed to the PSPC resolution, is significantly lower than A2125, but it is clear that the X-ray emission from A2645 is much more centrally condensed than A2125. This unusual property of A2125 is discussed in terms of a cluster-cluster merger by Wang, Connolly, & Brunner 1998, Roettiger, Burns, & Loken 1993.

In figures 3 and 4 we also include the positions of the radio galaxies reported here. One can see the

difference in the apparent density of radio objects and the correlation of the distribution in the A2125 with the extended optical and X-ray structures.

Although these clusters were picked to have very similar properties except for their blue fractions, a more detailed look reveals significant differences. First, A2125 appears to be a cluster merger in progress, as judged from the X-ray morphology (Wang, Connolly, & Brunner 1998) and the galaxy distribution. In contrast, A2645 appears to be centrally condensed and relatively relaxed. Its X-ray emission is also an order of magnitude stronger and much simpler than A2125. Using the count rate in the inner 500 kpc and correcting statistically to the entire cluster (Briel & Henry 1993), we find $L_x = 3.6 \times 10^{44} \text{ ergs s}^{-1}$ for A2645 and $3.7 \times 10^{43} \text{ ergs s}^{-1}$ for A2125. In figures 5 and 6, we show the X-rays as a greyscale with the adaptively smoothed optical galaxy contours overlaid (Beers et al, Morrison 1999). The adaptive kernel method is a two-step process. The initial smoothing scale is set at 0.5 Mpc at the redshift of the cluster. The final smoothing of the data is a function of the local galaxy surface density derived from the initial smoothing. The estimated background contribution to the galaxy surface density has been removed before plotting the optical contours with the lowest contour set to the estimated background level. One can see the excellent agreement between the X-rays and the optical galaxy counts.

In order to estimate the richness of the cluster to compare with other clusters, we counted galaxies down to a constant absolute magnitude as evaluated in the cluster's emitted frame, and within projected radii of 2 Mpc, $N_{2.0}$ (Abell 1958, Abell, Corwin & Olowin 1989), and 0.5 Mpc, $N_{0.5}$ (Bahcall 1981), assuming $H_0 = 75 \text{ km s}^{-1} \text{ Mpc}^{-1}$ and $q_0 = 0.1$. The limiting absolute magnitude was $M_R = -20.5$. This was determined by finding the absolute magnitude cutoff which agreed best with the Abell counts for a set of lower redshift, very rich clusters (Morrison 1999). Thus these results should be comparable with other richness estimates for clusters while being based on more consistent and quantitative selection techniques than Abell's approach.

We find $N_{2.0} = 278$ and 232 for A2125 and A2645, in agreement with the estimates of Abell 1958. However, we find $N_{0.5} = 42$ and 63 respectively. If we define the compactness as $C = N_{0.5}/N_{2.0}$, we find that A2645 is significantly more compact with $C = 0.27$, while A2125 has $C = 0.15$. This difference in concen-

tration is significant at the 99% level using a 2×2 contingency test. Inside the 0.5 Mpc radius we find a blue fraction for A2125 of $f_B = 0.20$ and for A2645 we find $f_B = 0.05$, in agreement with Butcher and Oemler (1984). See Morrison 1999 for details.

Thus, besides the difference in blue fraction, A2125 is much less compact than A2645 in both the X-ray and the optical bands. Figures 5 and 6 show this graphically. A2125 has two outlying clumps, consistent with the aftermath of a major merger while A2645 is much more compact and isolated as seen in both the X-ray gas and galaxy distributions.

6. Results for the Radio Galaxies

Several interesting differences between the populations in these clusters can be seen from tables 1 and 2. First, and most obvious, Abell 2125 has many more radio galaxies than Abell 2645. There are 27 radio galaxies associated with Abell 2125 compared with only four found in Abell 2645. Admittedly, our observations are more incomplete for A2645, but this cannot account for the difference. Within a circle 2.5 Mpc in diameter in projection at the cluster redshift, we have redshifts for all ID's brighter than $m_R = 19.5$ ($M_R = -21.0$), except for one object in A2125 and 5 in A2645. We find 25 confirmed cluster members for A2125 and only 2 for A2645. Thus if all the unmeasured objects in A2645 turn out to be cluster members, then we still find a large excess in A2125. From table 3, all four confirmed A2645 radio galaxies have radio luminosities $\geq 10^{23}$ W Hz $^{-1}$ while only 4 of the A2125 galaxies fall in this luminosity range. For A2645, all the confirmed cluster members exhibit old stellar populations, typical for their radio luminosities. Therefore the excess radio population in A2125 is entirely from lower-power objects, in the luminosity range $< 10^{23}$ W Hz $^{-1}$. This might suggest star formation as the dominant source of the excess in A2125. However, their optical spectra present a more complex picture.

In A2125, there is a clean color demarcation between objects with emission lines and pure absorption spectra, in the sense that all radio sources with observed $(B - R) < 1.6$ have emission lines and redder objects do not, suggesting that most of these objects have line emission directly related to the observable stellar populations and not, for example to AGN which are too weak to dominate the integrated colors. This also applies to the foreground and background

objects too, as it happens, though the interpretation of the color is rather different at the lower foreground redshifts. There are no galaxies in the redshift-culled A2645 sample blue enough to have emission lines by this criterion, and indeed none are observed to show emission lines. This demonstrates that the blue radio-source population is uniquely associated with events in A2125; the red population is numerically enhanced, while the blue one has appeared from nowhere in comparison.

In table 3, we have divided the A2125 cluster radio galaxies into four classes depending on their optical spectra. About half (13/27) are dominated by old stellar populations based on their colors and/or the 4000Å break. None of these systems have detected line emission. However, 8 of these galaxies have radio luminosities below 10^{23} W Hz $^{-1}$, a range normally associated with star-forming galaxies rather than traditional AGN. A second group of 5 have spectra consistent with vigorous star formation based on colors, D(4000) and emission lines. One object has emission line ratios consistent with AGN activity and a radio luminosity greater than is common for star forming objects. However, its small value of D(4000) suggests star formation as well.

The remaining 8 objects present the biggest puzzle. These objects all have some evidence of a younger stellar population, either from their color, low values of D(4000) or both. However, they have weak or undetectable line emission, which would in itself suggest weaker star formation than would their radio luminosities. In figure 7, we show the concentration index data from table 3. The plot shows that most of the old stellar population objects cluster near the de Vaucouleurs profile while the starforming objects are closer to the exponential disk curve. The intermediate objects are spread over the entire range, although four of the seven lie on the exponential disk curve. Thus most of the weak radio galaxies have optical properties which are most consistent with systems later than E/S0.

In table 4 we consider the origin of the radio emission by comparing the predicted star-formation rates (SFR) for the A2125 radio galaxies as based on $H\alpha$ +[NII] luminosity, [O II] luminosity and radio luminosity. We use the values from Kennicutt (1998) (corrected for 1.1 magnitudes of extinction at $H\alpha$) for $H\alpha$ and [O II]. For the radio SFR we use the relationship in Condon (1992). We plot the radio luminosity versus the line luminosities in figures 8 and 9.

The solid line indicates the prediction from Kennicutt (1998) and Condon (1992) for a constant SFR and the dashed lines the expected uncertainty due to the local dust obscuration variations. For $H\alpha+[NII]$ and $[OII]$ the obviously star-forming galaxies (with strong line emission, from Table 3 agree with the predictions from the radio. For all the other object classes, the radio flux density is stronger than predicted from the line luminosities.

Also one can see from table 4 that for the old stellar population objects, the radio-derived SFR is much larger than the limit we can set from the optical lines. This is consistent with the radio emission being driven by radio jet emission related to weak AGN's. For the stronger sources we can see extended radio jet structures which confirm this picture. For the sources weaker than $10^{23} \text{ W Hz}^{-1}$ we see unresolved sources consistent with weak FR I sources but which could, in principle, be very obscured star formation. But from the current evidence, these objects seem most consistent with FR I/weak AGN activity.

For the objects classified as starbursts, the agreement between the radio and optical SFR's is surprisingly good given the uncertainties in the calculations. Only 154040+661309 has some disagreement between the different techniques in the sense that the radio is too weak. This might be explained if the extinction is lower than assumed in this case and/or the star formation is concentrated to the core of the galaxy, since our estimate of the absolute luminosity assumes the EW is the same over the entire Gunn-Oke aperture.

For the Intermediate sample the answer is less clear but in most cases, the star formation rates do not disagree by factors larger than the corrections applied. For the four systems whose light distributions are consistent with disks, the disagreement with the $[O II]$ results are a factor of 3-5. The radio SFR for 154053+660526 agrees well with the $H\alpha$ luminosity. The three other objects which do not fit a disk-model well have no detected line emission, redder colors and larger $D(4000)$'s than the other objects and thus seem to be candidates for weak AGN's. However, in all cases, it is hard to make a strong case for either mechanism. We could be looking at weak AGN's, very obscured star formation or a mixture of the two. However, from the preponderance of the data we favor star formation as the origin the radio emission for most of these systems.

The AGN 154109+661544 stands out as a strong AGN. Alone among the radio sources we have ob-

served in A2125, it has a ratio of $[NII]/H\alpha$ line strengths consistent with an AGN instead of star formation. Its radio luminosity is clearly above the star-formation range and the radio prediction of the the SFR is 50 times higher than the line luminosities predict. However, its $D(4000)$ and color are very small and consistent with star formation as well as AGN activity or possibly with a very strong non-thermal component.

7. Discussion

The blue cluster Abell 2125 has a radio galaxy population below $10^{23} \text{ W Hz}^{-1}$ which is not found in the red comparison cluster, Abell 2645. Part of this population shows active star formation and lies preferentially on the outskirts of apparently merging clumps. However, most of this excess appears to be associated with galaxies with little or no evidence for star formation rates high enough to explain the radio emission. Two logical possibilities exist; either the excess radio emission is due to weak AGN activity, difficult to detect except from its radio emission, or the star formation activity is well hidden, probably by dust.

In either case the radio-galaxy population seems to be related to the current nature of the clusters. A2645 is much more X-ray luminous and seems to have a relatively simple structure resembling many cooling-flow clusters. A2125 appears to be in the middle of a violent merger. Hydrodynamic simulations have suggested that a cluster merger can disrupt a cooling flow and heat the X-ray gas, so that unusually weak X-ray emission could be a side effect of such an event (*e.g.* Gomez et al 1996, Roettiger, Stone, & Mushotzky 1998), although it is not clear whether this process is just beginning or is in its later stages (see *e.g.* Roettiger, Burns, & Loken 1993). This raises the question of whether the merger has anything to do directly with the radio excess. One might consider accretion of radio galaxies from the field, whose activity have not yet been snuffed out by the intracluster environment, but it is difficult to understand why we do not see such a population in the outskirts of A2645.

Another appealing possibility is that the cluster-cluster interaction has somehow enhanced the radio population, either through mutual galaxy interactions or through galaxy-ICM interaction. The question is how this might be happening in detail. If galaxy-galaxy mergers/interactions are responsible, where and how are the interactions taking place? Hyper-

bolic encounters one might expect in cluster-cluster merger are more likely to inhibit star formation, if local examples may be generalized (Combes et al (1988)). From figure 3 one can see that the starforming and intermediate radio galaxies mostly avoid the central X-ray/optical concentration. However, they follow the general outline of the of the extended cluster to the southwest, apparently lying on the outskirts of the overall distribution. Thus it seems likely that whatever mechanism is responsible for the radio emission takes place outside the dense cluster core. From the Las Campanas optical spectral survey, Hashimoto et al., (1998) find a higher probability of line emission from galaxies in intermediate density regions than in the dense cores of clusters or in the low density field. This could be due to the cross-section for galaxy-galaxy interactions being maximized in such an environment. Lavery, Pierce & McClure (1992) have pointed out the existence of a surprisingly large population of close, blue pairs among the blue populations in Butcher-Oemler clusters which may indicate some process for increased interactions between galaxies outside the cluster core. To increase galaxy-galaxy interactions, one needs regions with low relative velocities between galaxies and as high galaxy densities as possible. Such regions might occur in the outlying groups of each of the two subclumps which must also be undergoing group-group mergers. Whether these occur at low enough relative velocities is an open question. Another possibility is that a cluster-cluster merger simply correlates with a denser supercluster region which would maximize the galaxy-galaxy interaction rate. These issues probably require studies of simulations of cluster-cluster mergers to understand if any such process is taking place.

However, the lack of the star formation signature in the optical spectra of many of the radio galaxies might mean that AGN's as well as starbursts have been stimulated. The origin of AGN's is still unclear but it could be that AGN activity is another result of galaxy-galaxy interactions or mergers, perhaps with a different timescale (*e.g.* Wilson 1996). Many more clusters will need to be studied, and more detailed work on these clusters needs to be done, to explore the correlations and the physical picture suggested here. As a next step, we will present a more detailed study of the properties of the radio-loud and radio-quiet galaxies in A2125 in a subsequent paper.

8. Conclusions

1. The blue Butcher-Oemler cluster, A2125, has a large excess of radio galaxies relative to the red cluster, A2645, although both clusters have similar richnesses and redshifts.
2. This excess occurs for 20cm radio luminosities below 10^{23} W Hz⁻¹. Locally, radio galaxies at these luminosities are mostly driven by star-formation.
3. The optical properties of these radio galaxies are mostly consistent with systems later in type than E/S0. However, most have lower line luminosities than would be expected from their radio luminosity if star-formation is driving the activity. This result seems most consistent with enhanced extinction relative to most nearby systems obscuring the star-forming regions.
4. Besides A2125 blue galaxy population, the cluster appears to be in the process of a cluster-cluster merger which may be related to the unusual activity.

The authors wish to thank Elizabeth Rizza for obtaining the B image of A2645 for us with the KPNO 0.9m.

REFERENCES

- Abell, G. O. 1958, ApJS, 3, 211
- Abell, G. O., Corwin, H. G., & Olowin, R. P. 1989, ApJS, 70, 1
- Abraham, R. G., Valdes, F., Yee, H. K. C., & van den Bergh 1994, ApJ, 432, 75
- Bahcall, N. A. 1981, ApJ, 247, 787
- Beers, T. C., Forman, W., Huchra, J. P., Jones C., & Gebhardt, K. 1991, AJ, 102, 1581
- Briel & Henry 1993, A&A, 278, 79
- Burstein, D. & Heiles, C. 1981, ApJ, 87, 1165
- Butcher, H. & Oemler, A. 1984, ApJ, 285, 426
- Christian, C.A., Adams, M., Barnes, J.V., Hayes, D.S., Butcher, H., Mould, J. R., & Siegel, M. 1985, PASP, 97, 363
- Combes, F., Dupraz, C., Casoli, F., & Pagani, L. 1988, A&A, 203, L9
- Condon, J. J. 1992, ARA&A, 30, 575
- Dwarakanath, K. S. & Owen, F. N. 1996, in *Cold Gas at High Redshift*, (Bremer et al, eds.), Kluwer, p183
- Dwarakanath, K. S. & Owen, F. N. (1999), submitted
- Frei, Z. & Gunn, J. E. 1994, AJ, 108, 1476
- Gomez, P. L., Loken, C., Burns, J. O., & Roettiger, K. 1996, BAAS, 189, 11503
- Gunn, J.E. & Oke, J. B. 1975, ApJ, 195, 255
- Hashimoto, Y., Oemler, A., Lin, H., & Tucker, D. L. 1998, ApJ, 499, 589
- Kennicutt, R. C. 1998, ARA&A, 36, in press
- Landolt, A.U. 1983, AJ, 88, 439
- _____ 1992, AJ, 104, 340
- Lavery, R. J., Pierce, M. J., & McClure, R. D. 1992, AJ, 104, 2067
- Ledlow, M. J. & Owen, F. N. 1995, AJ, 110, 1959
- Morrison, G. E. 1999, PhD Thesis, University of New Mexico
- Newberry, M. V., Kirshner, R. P., & Boroson, T. A. 1988, ApJ, 335, 629
- Owen, F. N. 1996, in *Extragalactic Radio Sources, IAU 175*, Kluwer, (Ekers, Fanti, & Padrielli, eds.), p305
- Owen, F. N., Dwarakanath, K. S., Smith, C., Ledlow, M. J., Keel, W. C., Morrison, G. E., Voges, W., & Burns, J., 1996 in *Energy Transport in Radio Galaxies and Quasars*, (P. Hardee, A. Bridle, & A. Zensus, eds.), ASP Conference Series, Vol. 100, p. 353
- Owen, F.N., Ledlow, M.J., & Keel, W.C. 1995, AJ, 109, 14
- Owen, F.N. & Laing, R.A. 1989, MNRAS, 238, 357
- Roettiger, K., Burns, J. & Loken, C. 1993. ApJ, 407, L53
- Roettiger, K., Stone, J. M., & Mushotsky, R. F. 1998, ApJ, 493, 62
- Wang, Q. D., Connolly, & Brunner, R. J. 1997, ApJ, 487, L13
- Wilson, A.S. 1996, in *Energy Transport in Radio Galaxies and Quasars*, (P. Hardee, A. Bridle, & A. Zensus, eds.), ASP Conference Series, Vol. 100, p. 9

TABLE 1
OPTICAL IDS FOR ABELL 2125

R.A.(2000.0)	Dec(2000.0)	R(GO)	B-R	Redshift
15 39 08.82	66 08 54.4	(18.8)		0.2448(0.0003)
15 39 33.07	66 07 43.5	20.00	2.11(0.09)	
15 39 46.83	66 06 24.9	20.92		
15 39 59.33	66 11 26.7	18.71	1.43(0.05)	0.2457e(0.0003)
15 39 59.40	66 16 07.4	18.02	2.34(0.05)	0.2459(0.0003)
15 40 00.00	66 05 51.6	20.38	0.98(0.11)	
15 40 05.35	66 10 13.0	18.03	2.37(0.05)	0.2425(0.0003)
15 40 08.70	66 15 36.3	18.99	0.74(0.08)	0.0931(0.0003)
15 40 09.05	66 12 17.0	17.63	2.41(0.05)	0.2455(0.0003)
15 40 12.06	66 12 09.9	18.11	2.33(0.05)	0.2567(0.0003)
15 40 15.85	66 11 09.9	18.62	1.31(0.08)	0.2449(0.0003)
15 40 26.00	66 30 30.4	(18.5)		0.2573(0.0004)
15 40 30.13	66 12 14.3	19.08	1.79(0.05)	0.2458(0.0004)
15 40 30.23	66 13 06.3	18.15	2.23(0.05)	0.2496(0.0004)
15 40 30.91	66 12 26.3	19.50	1.35(0.06)	0.2458e(0.0003)
15 40 33.62	66 08 01.5	20.90	0.93(0.08)	
15 40 40.03	66 13 09.0	18.87	1.19(0.05)	0.2462e(0.0003)
15 40 40.83	66 26 54.2	16.46	1.56(0.07)	0.0564(0.0003)
15 40 42.55	66 08 54.2	20.48	1.82(0.28)	
15 40 43.18	66 10 20.8	20.08	1.77(0.16)	
15 40 49.18	66 18 39.7	18.52	2.21(0.05)	0.2433(0.0003)
15 40 50.98	66 16 32.2	18.34	1.56(0.05)	0.1277(0.0002)
15 40 51.80	66 06 31.0	18.43	2.55(0.06)	0.3640(0.0003)
15 40 53.64	66 05 26.4	19.43	1.65(0.10)	0.2527(0.0004)
15 40 54.51	66 11 27.5	19.53		
15 40 54.66	66 17 15.7	18.43	1.89(0.05)	0.2459(0.0003)
15 40 56.88	66 26 45.8	18.25	1.70(0.08)	0.2443(0.0003)
15 41 00.52	66 13 54.2	20.42	1.43(0.16)	
15 41 01.93	66 16 26.6	17.50	2.34(0.05)	0.2456(0.0003)
15 41 05.33	66 12 35.7	18.89	1.54(0.05)	0.2754e(0.0003)
15 41 07.29	66 21 23.9	20.81	0.75(0.15)	
15 41 09.73	66 15 44.5	18.75	1.23(0.05)	0.2526(0.0003)
15 41 10.63	66 13 13.9	19.93	1.71(0.14)	
15 41 14.38	66 15 56.8	17.26	2.37(0.05)	0.2520(0.0003)
15 41 14.60	66 21 39.9	16.58	1.27(0.07)	0.0855(0.0003)
15 41 14.85	66 16 03.6	17.29	2.37(0.05)	0.2470(0.0002)
15 41 15.36	66 15 58.9	17.80	2.41(0.08)	0.2466(0.0002)
15 41 28.12	66 13 23.6	17.34	0.81(0.05)	0.0931(0.0003)
15 41 33.91	66 22 54.7	19.55	2.31(0.16)	
15 41 33.98	66 31 11.3	(16.9)		0.2361(0.0004)
15 41 40.99	66 22 37.8	20.41	0.53(0.10)	
15 41 43.22	66 15 16.6	18.56	2.22(0.08)	0.2520(0.0003)
15 41 48.79	66 11 37.0	19.82	>2.0	
15 42 02.76	66 15 55.1	19.31	2.15(0.13)	0.2407(0.0003)

TABLE 1—*Continued*

15 42 03.88	66 26 31.7	19.14	2.13(0.11)	0.2464(0.0004)
15 42 14.67	66 30 04.0	(18.6)		0.2999(0.0004)
15 42 24.26	66 19 58.4	18.02	2.30(0.08)	0.2473(0.0003)
15 42 24.67	66 29 04.3	(19.3)		0.2999(0.0004)
15 42 25.06	66 09 17.3	20.94	1.16(0.21)	
15 42 41.09	66 24 36.9	18.08	0.97(0.07)	0.2757(0.0002)
15 42 41.44	66 24 33.7	18.37	0.81(0.07)	0.2748(0.0002)
15 43 01.07	66 15 16.9	19.92		
15 43 07.81	66 13 43.9	(19.3)		
15 43 44.83	66 30 01.0	(18.9)		0.2482(0.0004)

TABLE 2
OPTICAL IDS FOR A2645

R.A.(2000.0)	Dec(2000.0)	R(GO)	B-R	Redshift
23 40 27.82	-09 09 45.9	(15.6)		0.0728e(0.0001)
23 40 39.56	-08 51 37.1	20.11	2.19(0.09)	
23 40 43.18	-08 53 56.6	19.23	2.61(0.07)	
23 40 45.51	-09 01 55.0	19.61	2.47(0.08)	
23 40 49.39	-08 57 03.7	18.32	1.68(0.05)	
23 40 53.08	-09 03 15.3	18.86	0.62(0.05)	1.182e(0.0004)
23 40 53.22	-08 58 30.1	18.88	1.62(0.06)	0.2945e(0.0002)
23 40 57.04	-09 01 53.7	17.77	1.65(0.05)	0.1522(0.0003)
23 41 07.73	-08 55 45.8	19.99	1.61(0.07)	
23 41 10.19	-08 57 11.9	18.03	2.39(0.06)	0.2477(0.0003)
23 41 11.40	-08 44 47.5	(17.7)		0.2420(0.0004)
23 41 11.57	-09 02 02.2	18.39	2.48(0.06)	0.2518(0.0003)
23 41 13.04	-09 02 12.4	20.64	2.30(0.14)	
23 41 13.99	-09 07 47.8	18.93	2.50(0.06)	0.4422(0.0006)
23 41 15.28	-09 05 17.2	18.04	2.53(0.05)	
23 41 16.20	-08 55 09.6	19.64	1.60(0.06)	
23 41 17.11	-09 02 17.0	19.55	1.63(0.06)	
23 41 20.76	-08 55 42.1	18.78	1.63(0.05)	0.1724e(0.0002)
23 41 21.97	-09 02 13.5	18.63	1.31(0.05)	0.1071e(0.0002)
23 41 26.03	-09 04 50.3	17.44	1.90(0.05)	0.0713(0.0006)
23 41 37.33	-08 51 53.4	19.80	2.11(0.08)	
23 41 37.54	-09 11 00.0	20.09	> 3.6	
23 41 37.86	-09 04 11.7	20.38	> 3.3	
23 41 39.45	-09 02 11.4	17.40	1.90(0.05)	0.1539(0.0005)
23 41 39.61	-08 48 36.8	(19.0)		
23 41 40.65	-08 43 13.2	(16.1)		0.0739e(0.0001)
23 41 42.30	-09 14 32.3	(16.7)		0.0887(0.0002)
23 41 44.10	-09 08 00.4	19.80	2.70(.11)	
23 41 57.99	-08 55 16.2	17.19	2.33(0.05)	0.1742(0.0006)
23 41 59.74	-09 02 05.8	19.47	2.09(0.07)	
23 41 59.76	-09 03 48.5	16.91	2.17(0.05)	0.1529(0.0003)
23 42 00.31	-09 03 00.4	20.18	2.13(0.09)	
23 42 03.04	-09 04 25.5	17.68	1.90(0.05)	0.1741(0.0003)
23 42 03.30	-08 51 28.0	(19.1)		0.2533(0.0003)
23 42 04.94	-09 15 10.9	(17.8)		0.2145(0.00004)

TABLE 3
A2125 & A2645 RADIO GALAXY PARAMETERS

Source	M_R	B-R	D(4000)	$\log L_{20}$ ergs s ⁻¹	C.I.	μ
Old						
153908+660854	(-21.7)		2.13	24.96		
153959+661607	-22.48	2.42	1.98	24.13	0.53	22.74
154005+661013	-22.47	2.40	2.10	22.85	0.63	22.38
154009+661217	-22.87	2.48	1.96	22.79	0.62	22.89
154012+661209	-22.39	2.41	2.09	22.48	0.68	22.32
154026+663030	(-22.0)		2.18	22.58		
154049+661839	-21.98	2.44	2.05	24.36		
154101+661626	-23.00	2.46	2.12	22.47		
154114+661556	-23.24	2.51	2.12	23.64		
154114+661603	-23.21	2.54	2.21	22.87		
154115+661558	-22.70	2.46	2.18	24.35		
154133+663111	(-23.6)		2.03	22.89		
154224+661958	-22.48	2.35	2.08	22.45	0.61	22.29
Starburst						
153959+661126	-21.79	1.44	1.22	22.58	0.38	22.08
154015+661109	-21.88	1.42	1.27	22.66	0.48	22.27
154030+661214	-21.42	1.92	1.45	22.42	0.50	22.22
154030+661230	-21.89	1.77	1.51	22.33		
154040+661309	-21.63	1.26	1.22	22.30	0.37	22.19
Intermediate						
154030+661306	-22.35	2.24	1.93	22.32	0.62	22.51
154053+660526	-21.07	1.70	1.68	22.45	0.33	22.48
154054+661715	-22.07	1.89	1.99	22.63	0.49	22.51
154056+662645	-22.05	1.75	1.77	22.57	0.38	22.63
154143+661516	-21.94	2.27	1.86	22.38	0.58	22.54
154202+661534	-21.19	2.20	1.62	22.29	0.37	22.47
154203+662631	-21.36	2.17	1.43	22.66	0.34	22.40
154344+663001	(-21.6)		1.63	22.90		
AGN						
154109+661544	-21.75	1.15	1.23	24.53	0.42	22.18
A2645						
234110-085711	-22.48	2.67	1.95	23.00		
234111-084447	(-22.8)		1.96	24.02		
234111-090202	-22.12	3.19	2.27	23.59		
234203-085128	(-21.4)		2.11	23.27		

TABLE 4
A2125 STAR FORMATION ESTIMATES

Source	$\log L_{H\alpha}$ ergs s ⁻¹	SFR M_{\odot} yr ⁻¹	$\log L_{O[II]}$ ergs s ⁻¹	SFR M_{\odot} yr ⁻¹	$\log L_{20}$ W Hz ⁻¹	SFR M_{\odot} yr ⁻¹
Old						
153908+660854			< 40.35	< 0.9	24.91	2000
153959+661607	< 41.02	< 2.3	< 40.49	< 1.2	24.08	300
154005+661013			< 41.02	< 2.3	22.80	16
154009+661217	< 41.00	< 2.2	< 40.47	< 1.2	22.75	14
154012+661209	< 40.68	< 1.1	< 40.30	< 0.8	22.44	7
154026+663030	< 41.07	< 2.6	< 40.74	< 2.2	22.54	9
154049+661839	< 40.85	< 1.6	< 40.43	< 1.0	24.31	500
154101+661626			< 40.24	< 0.7	22.42	7
154114+661556			< 40.54	< 1.4	23.60	100
154114+661603	< 41.21	< 3.6	< 40.81	< 2.6	22.83	17
154115+661558			< 40.48	< 1.2	24.30	500
154133+663111			< 40.87	< 2.9	22.84	17
154224+661958			< 40.58	< 1.5	22.41	6
Starburst						
153959+661126	41.76	13	41.42	11	22.54	9
154015+661109	41.81	14	41.34	9	22.59	10
154030+661214	41.50	7	41.07	5	22.40	6
154030+661230	41.24	4	41.45	9	22.36	6
154040+661309	41.80	14	41.76	23	22.25	4
Intermediate						
154030+661306	< 41.04	< 2.4	< 40.46	< 1.1	22.28	5
154053+660526	41.25	4	40.66	1.8	22.41	6
154054+661715			< 40.51	< 1.3	22.58	10
154056+662645	< 40.96	< 2.0	< 40.61	< 1.6	22.53	8
154143+661516	< 41.17	< 3.3	< 40.51	< 1.3	22.33	5
154202+661534			40.39	1.0	22.24	4
154203+662631			40.82	2.6	22.61	10
154344+663001			40.49	1.2	22.85	18
AGN						
154109+661544	41.76	14	41.54	14	24.48	750

FIGURE CAPTIONS

Fig. 1.— Measured Redshift Distribution for A2125

Fig. 2.— Measured Redshift Distribution for A2645

Fig. 3.— R Image of A2125 with contours of X-ray intensity from ROSAT PSPC image overlaid. The X-ray image has been smoothed to a resolution of 250 kpc at the redshift of the cluster. The radio ID's have been marked on the image according to our spectral classification: Old stellar populations (circles), starbursts (7-pointed stars), intermediate (squares), and AGN's (diamonds). Two of the radio ID's in Table 3 are outside the image field-of-view (4.9 Mpc). Note that the central galaxy, near 154115+6616, is a triple system and each of the three optical nuclei is a separate radio source (see Dwarakanath & Owen 1999).

Fig. 4.— R Image of A2645 with contours of X-ray intensity from ROSAT HRI image overlaid. The HRI image has been regridded to match that of the PSPC, and smoothed to a resolution of 250 kpc. Three of the four radio ID's are marked on the image; the other is outside the field-of-view. All three radio ID's are old-population based on their spectra.

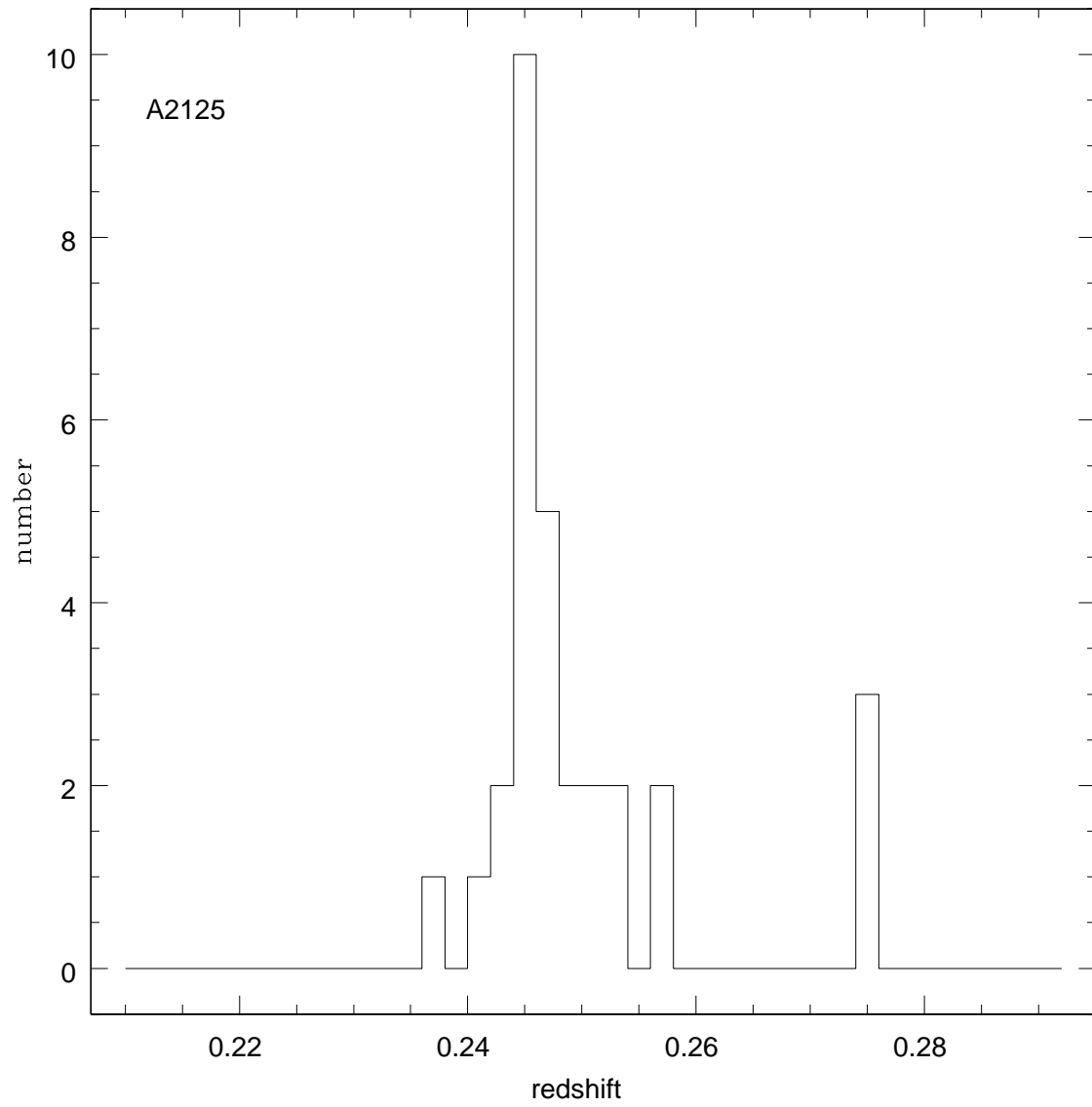
Fig. 5.— Adaptively Smoothed Contours of Galaxy Density overlaid on Greyscale of X-ray Intensity for A2125.

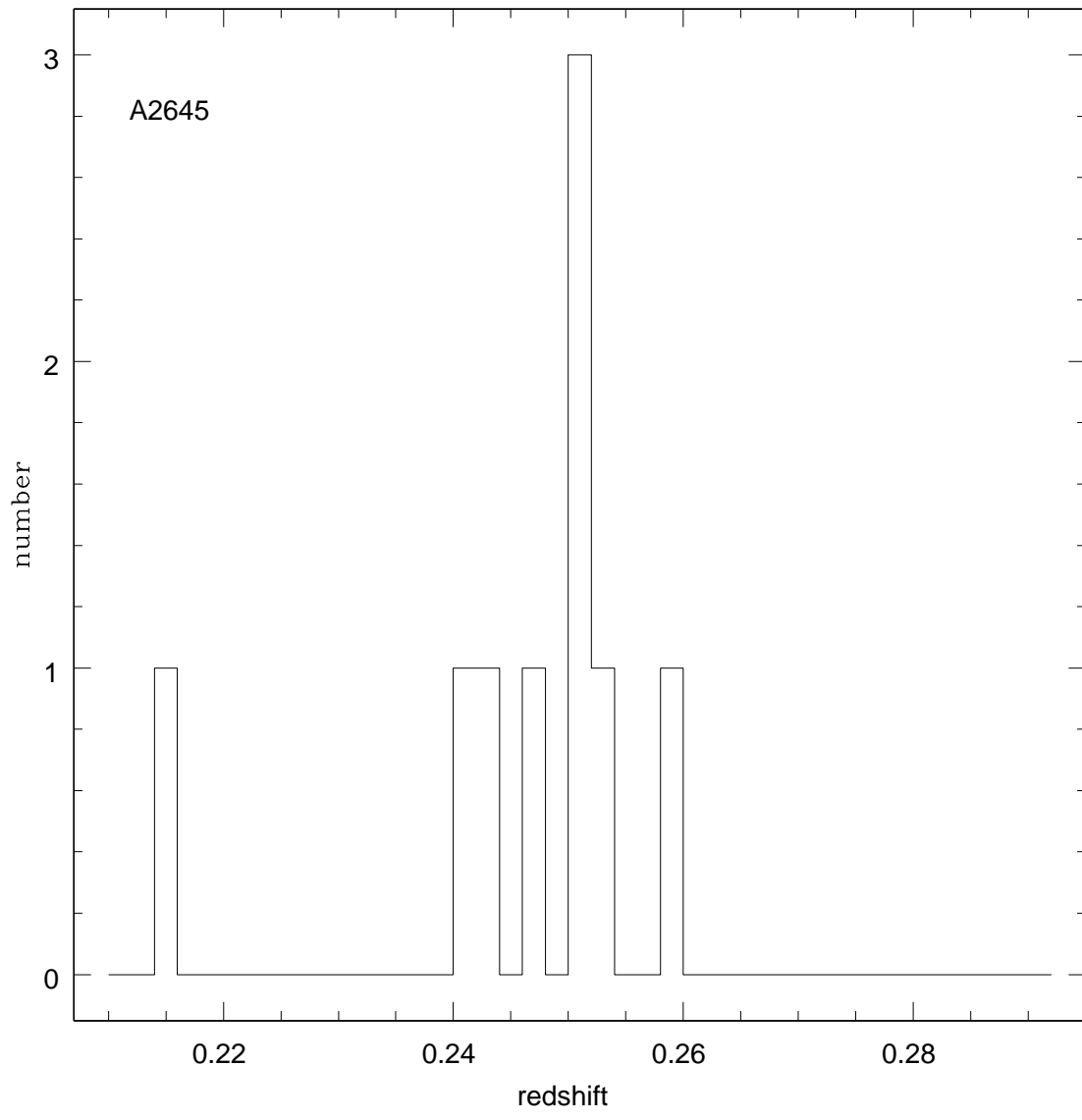
Fig. 6.— Adaptively Smoothed Contours of Galaxy Density overlaid on Greyscale of X-ray Intensity for A2645.

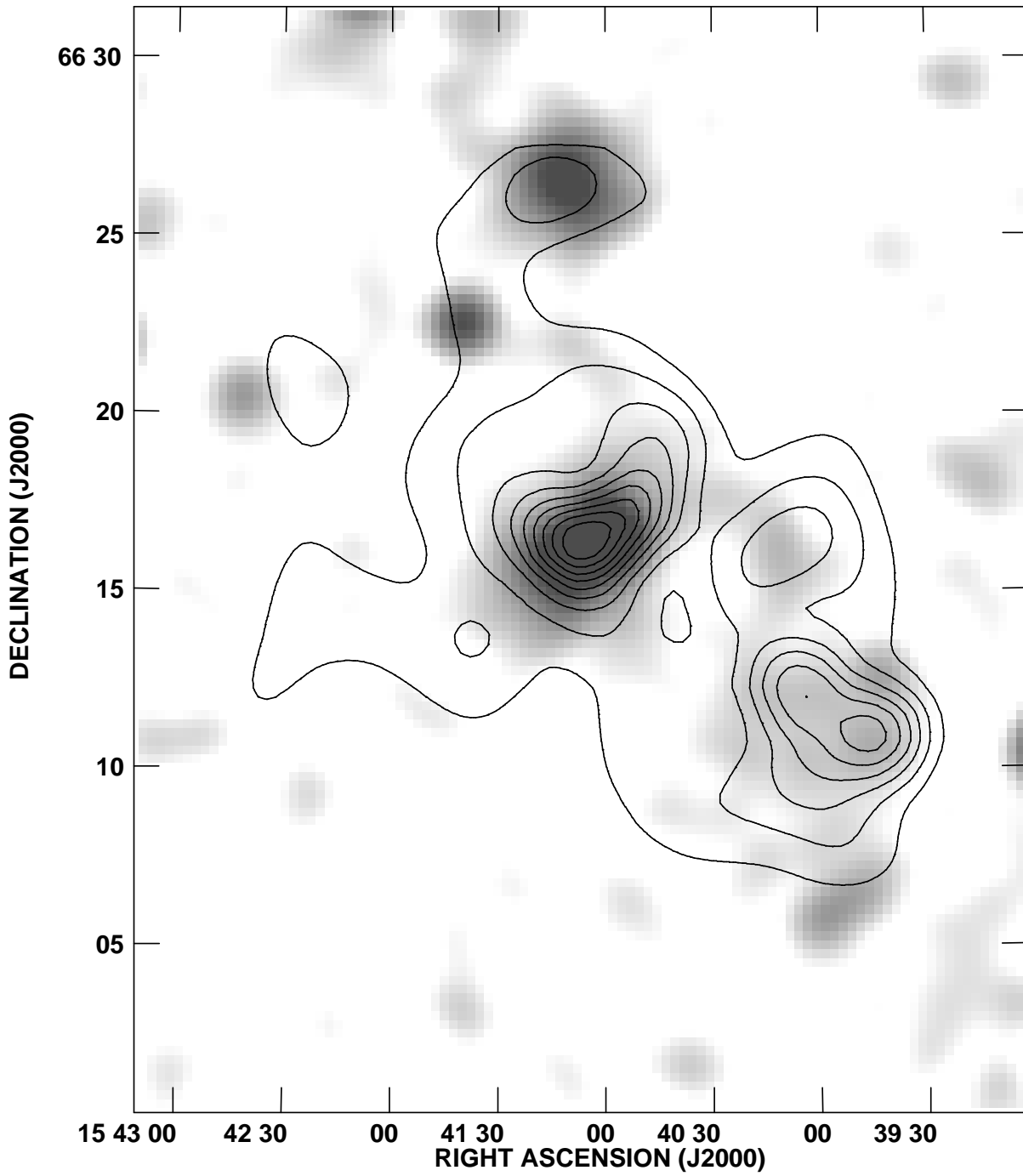
Fig. 7.— Surface brightness versus Concentration Index for fairly isolated galaxies. The symbols are as in figure 8. The solid line is the result for an exponential disk and the dotted line is for a de Vaucouleurs' $r^{1/4}$ law.

Fig. 8.— 20cm radio luminosity versus $H\alpha+[NII]$ luminosity for the A2125 radio galaxies in Table 3. The symbols represent the different classes: Old Population (O), Starbursts (S), AGN (A), and Intermediate (I). Lower-case letters indicate upper limits. The solid-line shows the result of combining the Condon (1992) and Kennicutt (1998) relations for the SFR assuming 1.1 magnitudes of dust extinction. The dashed-lines indicate the range of possible SFR's due to the uncertainty in the dust extinction (0.5 to 1.8 magnitudes).

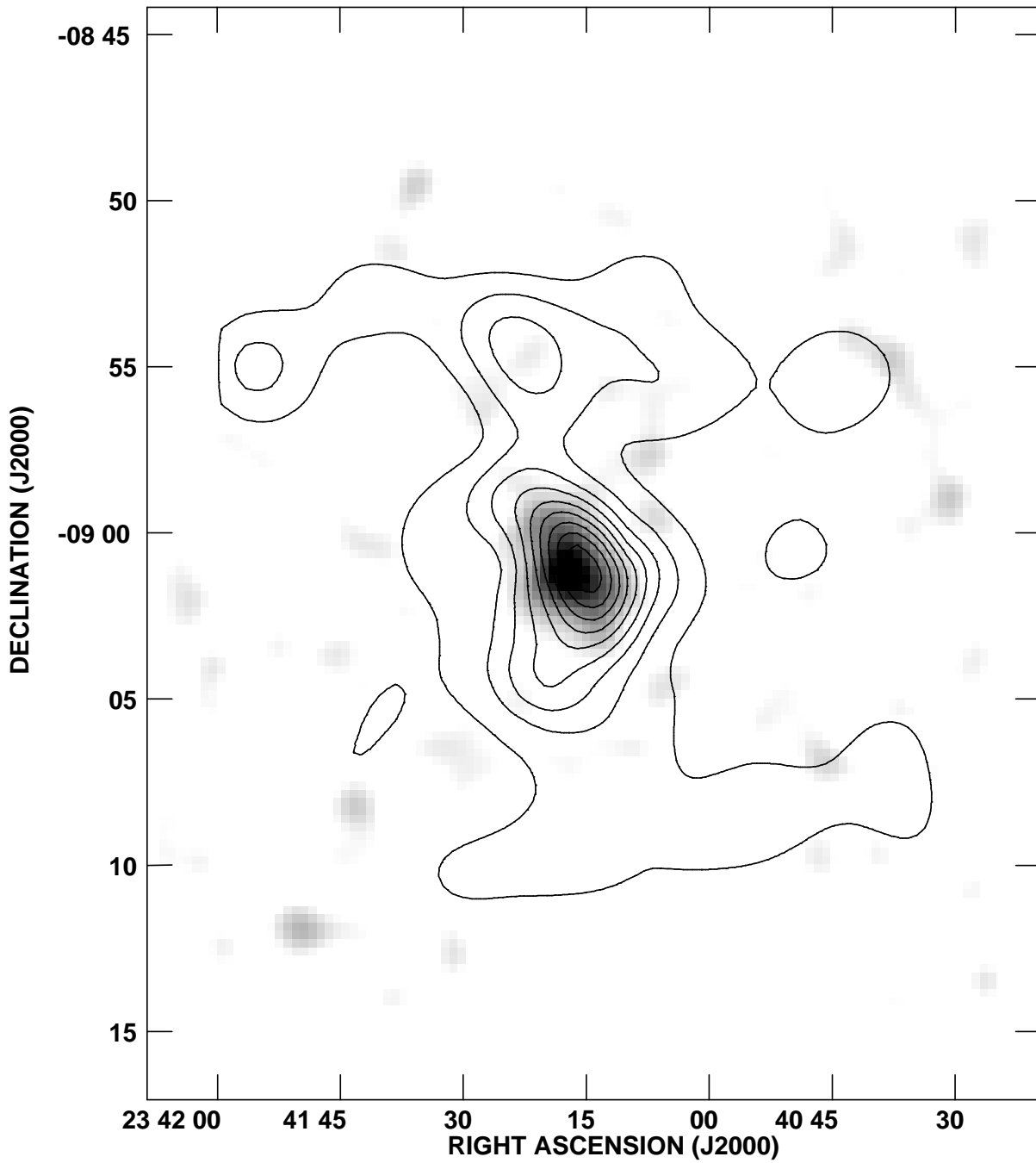
Fig. 9.— 20cm radio luminosity versus $[OII]$ luminosity. Labels and the line are as referenced in 8. The dashed-lines indicate both the uncertainty in the dust extinction (0.5-1.8 magnitudes) as well as an intrinsic scatter (28%) in the $[OII]$ SFR estimates (Kennicutt 1998).



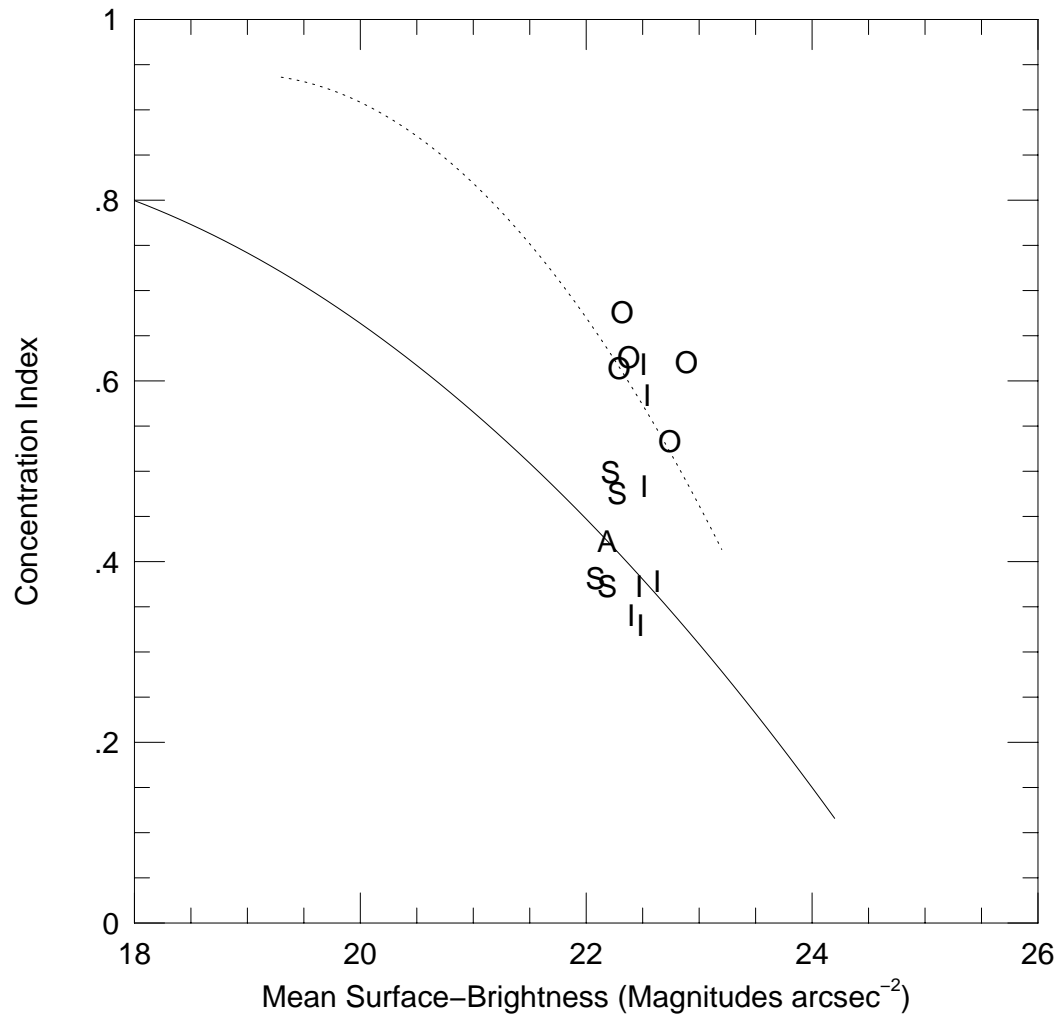


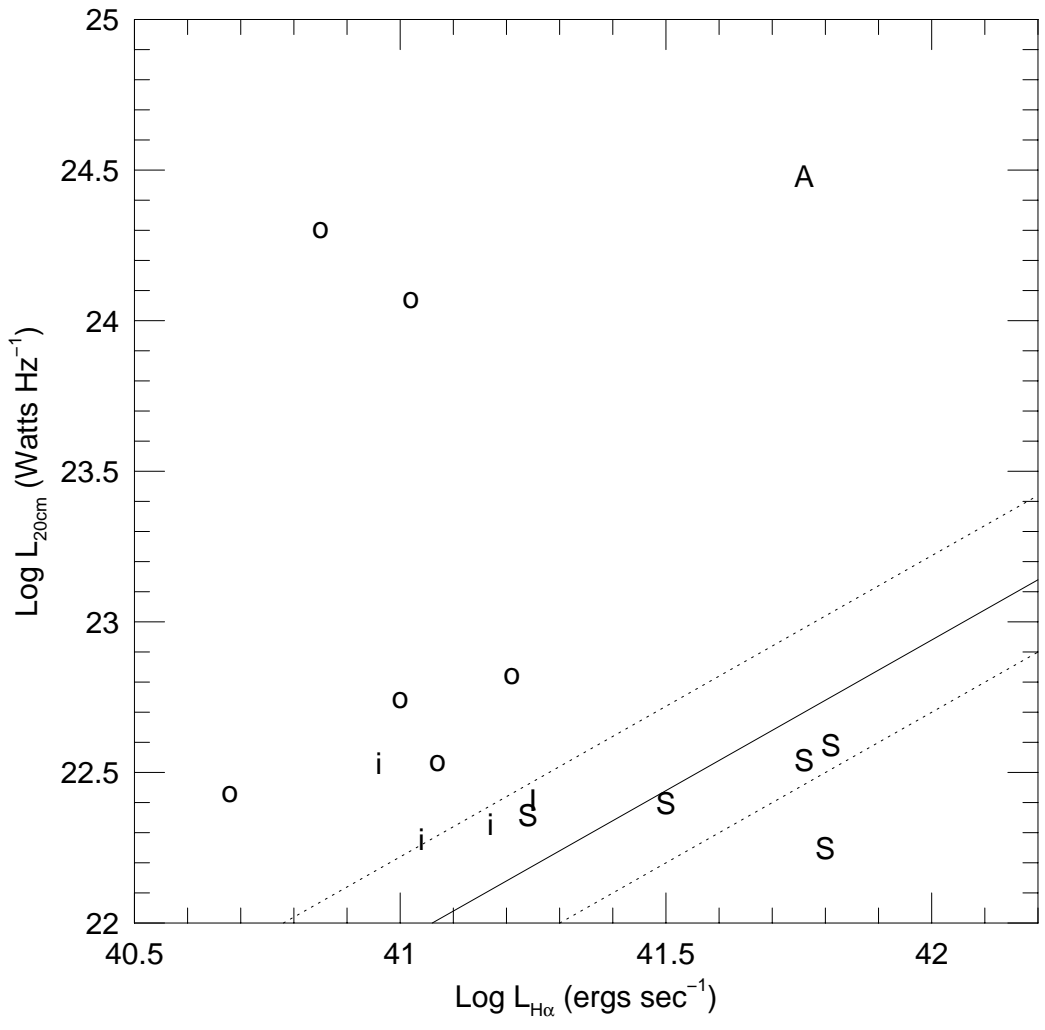


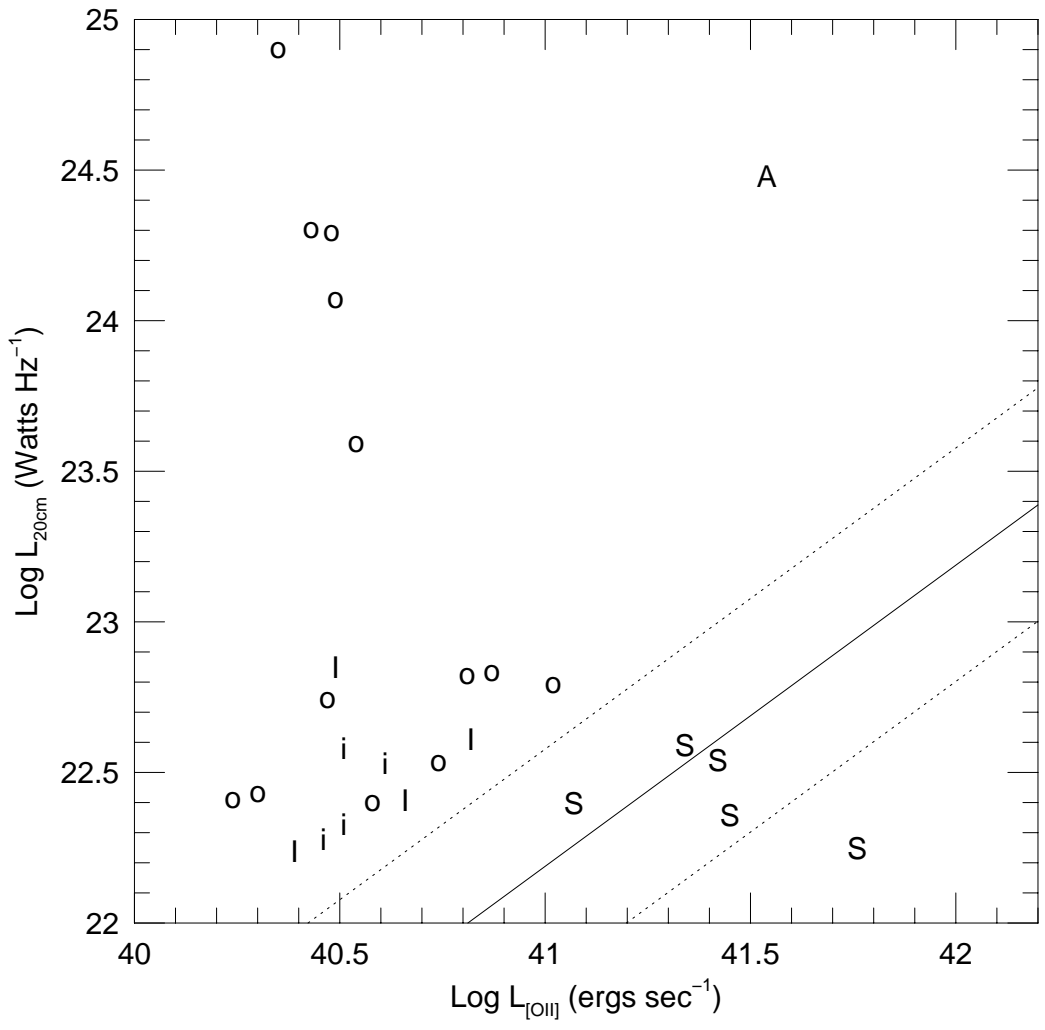
Cont peak flux = 8.3376E+00 GAL/SQAM
Levs = 8.3700E-01 * (1.000, 2.000, 3.000,
4.000, 5.000, 6.000, 7.000, 8.000, 9.000,
10.00)



Cont peak flux = 8.0966E+00 GAL/SQAM
Levs = 8.3700E-01 * (1.000, 2.000, 3.000,
4.000, 5.000, 6.000, 7.000, 8.000, 9.000,
10.00)







This figure "fig3.jpg" is available in "jpg" format from:

<http://arxiv.org/ps/astro-ph/9905004v1>

This figure "fig4.jpg" is available in "jpg" format from:

<http://arxiv.org/ps/astro-ph/9905004v1>